Essential Roles of Innersphere Metal Ions for the Formation of the Glutamine Binding Site in a Bifunctional Ribozyme†

Nick Lee and Hiroaki Suga*

Department of Chemistry, 657 Natural Sciences Complex, University at Buffalo, State University of New York, Buffalo, New York 14260-3000

Received May 30, 2001; Revised Manuscript Received July 27, 2001

ABSTRACT: Numerous studies on naturally occurring ribozymes have shown that the functional roles of metal ions in promoting RNA catalysis are diverse. Earlier studies performed on the in vitro selected aminoacyl-transferase ribozyme (ATRib) have revealed that a fully hydrated Mg^{2+} ion plays an essential role in catalysis [Suga, H., Cowan, J. A., and Szostak, J. W. (1998) *Biochemistry* 28, 10118−10125]. More recently, we have evolved this ATRib into a bifunctional ribozyme, called AD02 [Lee, N., et al. (2000) *Nat. Struct. Biol. 7*, 28−33]. This new ribozyme consists of two catalytic domains, the original ATRib domain and a new glutamine-recognition (QR) domain, and exhibits a function of charging glutamine to tRNA. Here we elucidate crucial roles of metal ions involved in the QR domain, that are distinct from those in the ATRib domain. The metal ions in the QR domain require innersphere coordinations, and both Mg^{2+} and Ca^{2+} can support catalysis. Extensive Tb^{3+}−Mg^{2+} and Tb^{3+}−$Co(NH_3)_6^{3+}$ competition cleavage experiments have shown that the QR domain has high and low affinity metal binding sites, which are involved in the Mg^{2+}-dependent structural alteration to form the glutamine binding site [Lee, N., and Suga, H. (2001) *RNA 7*, 1043−1051]. Kinetic studies in the presence of divalent and monovalent ions have suggested that the essential role of the metal ions in the QR domain is most likely structural.

In the past decade, in vitro selection and directed evolution of RNA molecules have yielded a number of novel ribozymes (*1*−*5*) that are not seen in modern biological systems. The isolation of such ribozymes has extended the spectrum of reactions that can be catalyzed by RNA, showing that their catalytic repertoire is far greater than the phosphodiester transfer reaction catalyzed by the majority of natural ribozymes. We have previously used this technique to isolate a novel ribozyme, called AD02 (*6*), which consists of two distinct catalytic domains (Figure 1A), glutamine-recognition (QR)[1] and acyl-transferase (ATRib) domains, and catalyzes the two sequential steps of aminoacylation to exhibit an aminoacyl-tRNA synthetase-like function (Figure 1B). In the closed state, the QR domain charges L-glutamine cyanomethyl ester (biotin-L-Gln-CME) to the 5′-hydroxyl (5′-OH) group of the ATRib domain, where an internal loop (L6b) docks onto the internal guide sequence (IGS). Subsequently, the ribozyme rearranges to the opened state, which allows the IGS to interact with a transfer RNA (tRNA), and the 5′-glutaminyl (5′-Gln) group is transferred to the 3′-end of tRNA (Figure 1B).

We have previously defined the essential catalytic core of the QR domain by extensive biochemical probing, NAIM (nucleotide analogue interference mapping), mutational analysis, and structural minimization (*7*). The minimized structure is a 29-nt RNA consisting of the lower half of P6a and the P6b−L6b region (C103−G129, highlighted in bold letters in Figure 1A), and this mini-helix−loop RNA is capable of glutaminylating the 5′-OH group of ATRib in trans. On the basis of biochemical studies on AD02, we have proposed that a dynamic structural alteration occurs in the core of P6b upon L6b docking onto the IGS, thus allowing the formation of the Gln binding site.

Our previous studies (*8*−*10*) have shown that $ATRib^{trans}$ as an independent ribozyme (Figure 1A) is able to use both Mg^{2+} and $Co(NH_3)_6^{3+}$, suggesting that the outersphere interactions of a single metal ion (via water or ammonium ligands) with the ribozyme are responsible for activity. More recent studies described in the preceding paper in this issue (*11*) have defined a potential metal binding site consisting of G1−G2/U75−U76 and A41−U42. Since the AD02 ribozyme is bifunctional relying on both ATRib and QR domains, we wondered whether the QR domain has a distinct catalytic metal ion from the ATRib domain. Here we report extensive biochemical studies that focus on characterizing the role of the metal ion in the glutaminylation step and its potential binding site.

EXPERIMENTAL PROCEDURES

General Method for the Preparation of Ribozyme. The ribozyme was synthesized by T7 RNA polymerase runoff

† This research was supported by ACS PRF-33938-G4 and NSF MCB-9982237 to H.S.

* To whom correspondence should be addressed. E-mail: hsuga@acsu.buffalo.edu; phone: 716-645-6800, ext. 2170; fax: 716-645-6963.

[1] Abbreviations: AD02, ambidextrous ribozyme clone 2; ATRib, acyl-transferase; biotin-L-Gln-CME, biotinylated L-glutamine cyanomethyl ester; CHES, 2-[*N*-cyclohexylamino]ethanesulfonic acid; CMCT, 1-cyclohexyl-3-[2-morpholinomethyl]carbodiimide metho-*p*-toluenesulfonate; DEPC, diethyl pyrocarbonate; EDTA, ethylenediaminetetraacetic acid; EPPS, 4-[2-hydroxyethyl]-1-piperazinepropanesulfonic acid; IGS, internal guide sequence; MES, 2-[*N*-morpholino]ethanesulfonic acid; NAIM, nucleotide analogue interference mapping; PAGE, polyacrylamide gel electrophoresis; PCR, polymerase chain reaction; PIPES, piperazine-*N*,*N*′-bis[2-ethanesulfonic acid]; QR, glutamine-recognition.

10.1021/bi011103c CCC: $20.00 © 2001 American Chemical Society
Published on Web 10/18/2001

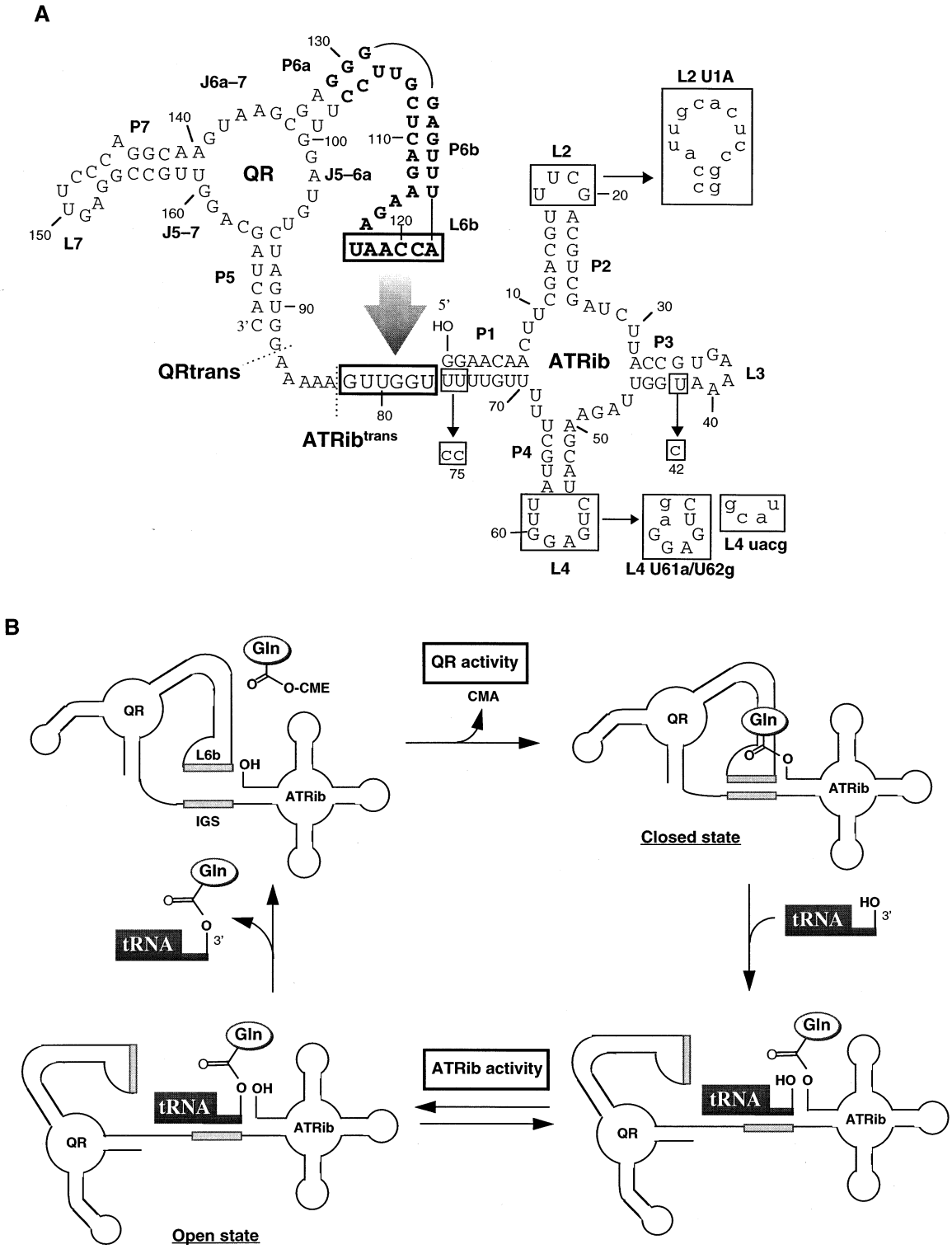

FIGURE 1: The AD02 ribozyme and its catalysis in tRNA aminoacylation. (A) Secondary structure of AD02. The ATRib (acyl-transferase ribozyme) domain consists of three stems (P1−3), three connecting internal loops (L2−L4), and an internal guide sequence (IGS). The QR (glutamine recognition) domain is composed of three major stems (P5, P6a−b, and P7) and two internal loops (L6b and L7). The base pair interaction between IGS and L6b, which are highlighted in thick line boxes, are indicated by a large arrow. Five adenosines connecting the two domains can be removed, generating QRtrans and ATRib^{trans}, where QRtrans trans-glutaminylates the 5′-OH of ATRib^{trans}. Essential catalytic residues of QRtrans are highlighted in bold. Single and double C-mutations in P3 and P1, respectively, and substitutions of L2 and L4 with the corresponding loops are highlighted in boxes, in which mutated bases are shown in lower case letters. (B) Schematic representation of AD02-catalyzed tRNA (or RNA) aminoacylation. The IGS and P6b regions are shown in thick lines. The acceptor tRNA, whose 3′-end sequence is complementary to IGS, is shown in thick line. The conformational rearrangement is induced by thermocycling in order to facilitate competition between the intermolecular IGS-tRNA and the intramolecular IGS-L6b interactions. CME and CMA denote cyanomethyl ester and alcohol, respectively.

transcription of a PCR-DNA template either in the absence or presence of α-[^{32}P]-UTP. After RNase-free DNase treatment for 15 min, the transcript was purified by 6% denaturing polyacrylamide gel electrophoresis (PAGE). The purified

RNA was dephosphorylated by calf intestinal phosphatase for 1 h, and the desired RNA was isolated by phenol−chloroform extraction and ethanol-precipitation. The pellet was then resuspended in DEPC (diethyl pyrocarbonate) water and stored at −20 °C.

Construction of ATRib^{trans} and QRtrans. For ATRib^{trans} mutants, the DNA template coding for ATRib^{trans} (*6*) was amplified by PCR in the presence of appropriate primers that introduce the desired mutations. For QRtrans, the PCR-DNA template of AD02 ribozyme was first passed through G-50 Sephadex columns (Boehringer Mannheim) to remove the wild-type primers that remained from the PCR reaction. The purified DNA was then used for PCR to generate the QRtrans DNA in the presence of the corresponding internal 5′-primer (containing T7 promoter sequence) and the 3′-primer.

End-Radiolabeling of Ribozyme. The unlabeled full-length AD02 ribozyme, prepared by the general RNA preparation method, was labeled by γ-[^{32}P]-ATP using T4 polynucleotide kinase (Promega) to yield 5′-[^{32}P]-labeled AD02. For 3′-end-labeling, unlabeled AD02 was treated with DNA Klenow fragment DNA polymerase I (Promega) in the presence of α-[^{32}P]-dATP, as described by Huang and Szostak (*12*).

Metal-Mediated Cleavage Reactions. A mixture consisting of a trace amount of the end-labeled RNA and an excess amount of the unlabeled RNA (a total of 1 μM) was dissolved in EK buffer (50 mM EPPS, 50 mM KCl, pH 7.5), denatured at 95 °C for 1 min, and slowly cooled to 25 °C for 5 min. The RNA was then equilibrated in the presence of 100 mM $MgCl_2$ at 25 °C for 3 min. Lead- and terbium-mediated cleavage reactions were initiated by either adding freshly prepared $Pb(OAc)_2$ or $TbCl_3$ solution with various final concentrations (0.03, 0.06, 0.12, 0.25, 1.0, 2.0 mM), and reaction samples were incubated at 25 °C for 1 h. Reactions were quenched with 80 mM EDTA, and the resulting RNA samples were ethanol-precipitated twice. Cleavage products were resolved by 8 and 10% PAGE and quantified using the Molecular Imager FX (Bio-Rad). For $Tb^{3+}-Mg^{2+}$ and $Tb^{3+}-Co(NH_3)_6^{3+}$ competition assays, experiments were conducted in a manner similar to the above experiment with the following modifications: To RNA samples in EK buffer, various amounts of $MgCl_2$ (0−100 mM) or $Co(NH_3)_6^{3+}$ (0−1.0 mM) were added and allowed to equilibrate at 25 °C for 3 min. Cleavage reactions were initiated by addition of 50 μM $TbCl_3$ and incubated at 25 °C for 1 h.

General Kinetic Assays. Cis-reactions were carried out as follows: A total of 8 μL of ribozyme solution was prepared by mixing 1 μL of 10 μM ribozyme, 2.5 μL of EK buffer (pH 7.5 or 8.0), and 4.5 μL of DEPC water. The RNA solution was heated at 95 °C for 1 min and cooled to 25 °C over 5 min. To this solution was added 1 μL of 500 mM $MgCl_2$ or $CaCl_2$ (giving a final concentration of 50 mM), and the mixture was equilibrated at 25 °C for 3 min. For glutaminylation (QR activity), reactions were initiated by the addition of 1 μL of 20 mM biotinylated L-Gln cyanomethyl ester (biotin-L-Gln-CME) to the ribozyme solution. For the aminoacyl-transfer reaction (ATRib activity), reactions were initiated by the addition of 1 μL of 50 μM biotin-L-Met-3′-ACCAAC-5′ to the ribozyme solution, similar to the procedure reported elsewhere (*9*, *10*). Aliquots were removed at various times, quenched with 80 mM EDTA, and ethanol-precipitated twice, and the pellets were resuspended in 4 μL of MEUS buffer (25 mM MOPS, 5 mM EDTA, 8 M urea, 10 μM streptavidin, pH 6.5). The resulting products were resolved by 6% PAGE at 4 °C and quantified using the Molecular Imager FX. Velocities were determined by talking at least six points from the linear regions of the time course and fitted using the KaleidaGraph graphing and curve-fitting package (Abelbeck Software). Trans-reactions were carried out in a similar manner as described above, except that the ribozyme solution was prepared by mixing 1 μL of 30 μM QRtrans, 1 μL of 20 μM [^{32}P]-body-labeled ATRib^{trans}, 2.5 μL of EK buffer at pH 7.5, and 3.5 μL of DEPC water.

Metal Ion-Dependent Kinetics and Co(NH$_3$)$_6^{3+}$ Inhibition. 100 mM divalent metal chloride solutions (Ca^{2+}, Mn^{2+}, Co^{2+}, Cu^{2+}, Zn^{2+}, and Cd^{2+}) in DEPC water were freshly prepared prior to set up the following experiments. The ribozyme solution containing 50 mM divalent metal ion was prepared as described in the general kinetic assays, except that the $MgCl_2$ solution was replaced with a divalent metal chloride solution. A stock of NaCl or KCl solution was prepared as a 4 or 1.6 M solution containing 2 mM EDTA. For the monovalent metal ion-dependent assays, the ribozyme solution was prepared by mixing 0.25 μL of 40 μM ribozyme, 2.5 μL of buffer (200 mM EPPS, pH 7.5), and 6.25 μL of 4 or 1.6 M monovalent solution. A 4 M NaCl stock solution containing 2 mM EDTA was diluted with DEPC water to prepare various concentrations of NaCl solution prior to the $Mg^{2+}-Na^+$ competition assay. The ribozyme solution was prepared in a manner similar to the monovalent metal ion-dependent assays, except that 2.5 μL of EK buffer at pH 7.5, 0.4 μL of $MgCl_2$, and 5 μL of various concentrations of NaCl solution were used instead. Prior to the $Co(NH_3)_6^{3+}$ inhibition assay, a 100 mM $Co(NH_3)_6^{3+}$ stock solution containing 1 mM EDTA was serially diluted with DEPC water to prepare various concentrations of $Co(NH_3)_6^{3+}$ solution. The ribozyme solution was prepared in a manner similar to the general kinetic assays, except that 3.5 μL of DEPC water was used instead of 4.5 μL, giving a total of 7 μL of solution. To this ribozyme solution was simultaneously added 1 μL of various concentrations of $Co(NH_3)_6^{3+}$ solution and 1 μL of 500 mM $MgCl_2$. The remaining procedures were the same as the general kinetic assays.

pH-Dependent Kinetics. Buffers were MES (pH 5.5−6.5), PIPES (pH 6.5−7.5), EPPS (pH 7.3−8.7), and CHES (pH 8.6−10). An 8 μL of RNA solution was prepared in a manner similar to the general kinetic assays, except that the EPPS buffer was replaced with the appropriate buffer to achieve the desired pH. After the RNA folding procedure, 1 μL of 500 mM $MgCl_2$ or 200 mM $CaCl_2$ was added. For the assays in the presence of spermidine, 1 μL of 100 mM $MgCl_2$ or $CaCl_2$ containing 20 mM spermidine was added to the folded RNA solution. The remaining procedures were carried out as described in the general kinetic assays.

RESULTS AND DISCUSSION

Metal Ion Dependence. Since the QR domain of the AD02 ribozyme was evolved in the presence of Mg^{2+} and K^+, the self-glutaminylation activity might rely on these metal ions. Our earlier study revealed that lowering the concentration of K^+ does not affect the catalytic rate (data not shown), thus suggesting that K^+ is not an essential component for catalysis. On the other hand, lowering the Mg^{2+} concentration

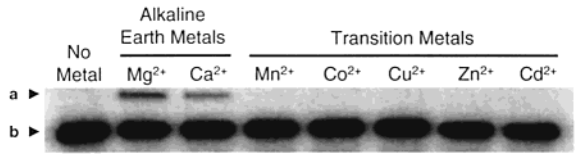

FIGURE 2: Divalent metal ion dependence of 5′-glutaminylation (QR activity). Cis-reactions were carried out in the presence of 50 mM metal (II) chloride, in 50 mM KCl and 50 mM EPPS, pH 7.5, for 1 h. The self-glutaminylated AD02 was resolved from the unreacted AD02 by streptavidin (SAv)-dependent gel mobility-shift assay. The arrowhead shows: a, biotin-Gln-AD02 complexed with SAv; b, AD02.

notably decreases the activity (vide infra). Therefore, we first attempted to uncover the scope of metal ion specificity by substituting Mg^{2+} with various divalent metal ions (Figure 2).

Among seven divalent metal ions tested, only the alkaline earth metal ions (Mg^{2+} and Ca^{2+}) are able to assist catalysis, whereas none of the tested transition metal ions, including Mn^{2+}, exhibits activity (Figure 2). A lack of activity observed for Mn^{2+} is a striking contrast to the metal dependence observed for naturally occurring ribozymes (*13*−*17*) (Mn^{2+} often supports catalysis to a certain extent), and also an interesting contrast to the metal dependence observed for the ATRib's function where Mn^{2+} can modestly support catalysis (*10*). Thus, the result suggests a unique role of the alkaline earth metal ion for the catalytic function of the QR domain.

To gain more insight into the Mg^{2+} preference, the initial rate constant was determined as a function of the Mg^{2+} ion concentration (Figure 3A). The titration plot ([Mg^{2+}] vs k_{obs}) displays a biphasic behavior; the activity initially increases according to a sigmoid-like curve below 20 mM, but above 20 mM it behaves linearly. This cooperative behavior can be ascribed to the involvement of multiple Mg^{2+} ions in the active form of the ribozyme. Since nonspecific Mg^{2+} often plays a role in shielding negative charges of phosphate backbone to avoid their unfavorable repulsion, to distinguish the catalytically essential Mg^{2+} ion(s) from a such non-specific one(s), we attempted to replace the latter Mg^{2+} ion-

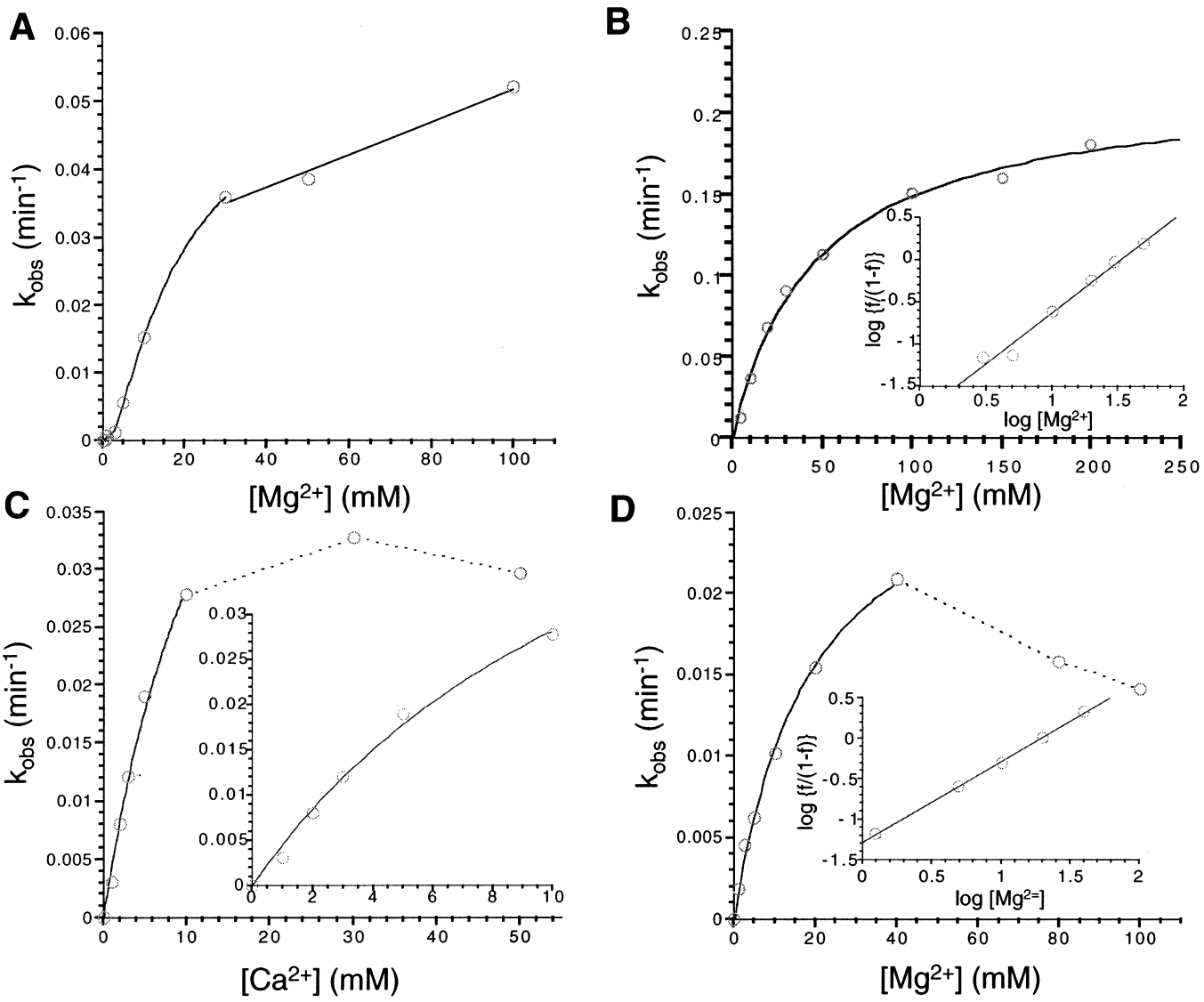

FIGURE 3: Catalytic activity of AD02 (cis-acting) as a function of divalent metal ion concentration at pH 8.0. (A) The Mg^{2+}-stimulated QR activity in the absence of spermidine. (B) The Mg^{2+}-stimulated QR activity in the presence of 2 mM spermidine. The inset shows a Hill analysis of the data below 100 mM Mg^{2+}, in which f represents fraction of activity at saturating Mg^{2+}. (C) The Ca^{2+}-stimulated QR activity in the presence of 2 mM spermidine. The inset shows a Hill analysis of the data below 10 mM Ca^{2+}. (D) The Mg^{2+}-stimulated ATRib activity in the presence of 2 mM spermidine. The inset shows a Hill analysis of the data below 40 mM Mg^{2+}.

(s) with spermidine (*10*, *18*−*20*). In the presence of 2 mM spermidine, the Mg^{2+}-titration data fit well to a single-site saturation-like curve (Figure 3B), where the dissociation constant for Mg^{2+} ($K_d^{Mg^{2+}}$) and maximal rate constant (k_{obs}^{max}) are determined to be 45.7 mM and 0.218 min^{-1}, respectively. However, Hill analysis of these titration data yields a slope of 1.20 ± 0.05 (inset in Figure 3B). Hence, the observed Hill coefficient indicates that more than one metal ion is likely required for the QR-domain-dependent self-glutaminylation (hereafter called QR activity).

The Ca^{2+}-titration data in the presence of 2 mM spermidine are similar to the Mg^{2+}-titration data but fit a saturation curve only at concentrations below 10 mM (Figure 3C). Above 10 mM, the activity slowly increases up to 30 mM and gradually decreases beyond 30 mM. Although the nature of this inhibitory behavior at high Ca^{2+} concentrations remains unclear, our results clearly display the unique role of the catalytic Mg^{2+} ion for the ribozyme function. It is noteworthy, however, that the catalytic rate below 10 mM Ca^{2+} is comparable with that of Mg^{2+} (more insight into this observation is discussed in the section *pH-Dependent Activity of Self-Glutaminylation*).

The Hill coefficient of 1.2 led us to hypothesize that multiple Mg^{2+} ions bind to the AD02 ribozyme. Previous studies on $ATRib^{trans}$ have revealed that a single metal ion is required for catalysis and its $K_d^{Mg^{2+}}$ is 14.0 ± 1.5 mM (*10*). We therefore wondered whether $K_d^{Mg^{2+}}$ of the ATRib domain in the AD02 ribozyme was similar, i.e. whether the catalytic Mg^{2+} in the ATRib domain still binds to the same site. To monitor the specific activity of ATRib domain, we utilized biotin-L-Met-3′-ACCAAC-5′ as a substrate and measured the initial rate constant for the "reverse" acyltransferase activity (*6*) as a function of the Mg^{2+} ion concentration in the presence of 2 mM spermidine. The titration data fit well to a saturation-like curve below 40 mM, but the activity was notably diminished above 40 mM (Figure 3D). It should be recalled that $K_d^{Mg^{2+}}$ for the QR activity is approximately 45 mM and the QR activity relies on docking of L6b onto IGS, which is the substrate binding site for the ATRib domain. Hence, the decline of k_{obs} can be attributed to an increase in the population of the closed state (i.e., docking of L6b onto IGS) over the open state (i.e., the active state for the ATRib domain) with increasing the concentration of Mg^{2+} (Figure 1B), thus resulting in inhibition of the ATRib activity.

The saturation-like fit below 40 mM in Figure 3D allows us to estimate $K_d^{Mg^{2+}} = 19.2 \pm 2.3$ mM, and the Hill analysis of this region yields a slope of 1.00 ± 0.05 (inset in Figure 3D). The similar $K_d^{Mg^{2+}}$ values observed for $ATRib^{trans}$ and the ATRib domain in AD02 as well as the requirement of a single metal ion suggest that the metal binding site in the ATRib domain remains largely unchanged. However, this $K_d^{Mg^{2+}}$ value for the ATRib activity is approximately 2.5-fold lower than that for the QR activity. The fact that there is a difference between the $K_d^{Mg^{2+}}$ values for ATRib and QR activities implies that the AD02 ribozyme has multiple metal binding sites. This view is indeed consistent with the requirement of more than one Mg^{2+} ion for the QR activity as seen in the Hill analysis (inset of Figure 3B).

It should be noted again that the AD02 ribozyme has two conformational states: In the closed state the QR domain is active, whereas in the open state the ATRib domain is active (Figure 1B). To monitor the specific activity of each conformation, we performed the metal-titration experiments using the substrate specific to each domain's activity (biotin-Gln-CME or biotin-Phe-3′-ACCAAC-5′). Even so, it is difficult to completely separate one conformer from the other since the formation of each substrate binding site is dependent upon the internal IGS−L6b interaction. The analysis of Mg^{2+}-dependent activity would be even more complicated when the formation of each substrate binding site could be Mg^{2+}-dependent, as seen in the Figure 3D. The pH-dependent kinetics of the QR domain-dependent self-aminoacylation (vide infra) have suggested that its chemistry is most likely rate-limiting at high concentrations of metal ion, and therefore the apparent affinity and cooperativity of Mg^{2+} monitored in the region of high Mg^{2+} concentrations in Figure 3B are a result of the Mg^{2+}-dependent chemistry of the QR domain. However, it is still possible that the rate-limiting step changes when the metal concentration decreases. Therefore, more detailed kinetics are necessary to better understand the rate-limiting step at lower concentrations of metal ion. Nonetheless, the critical information obtained by the series of metal-titration experiments is the possibility for the involvement of multiple metal ions in QR-dependent self-aminoacylation.

Location and Number of Metal Ions in the QR Domain. The hydrolytic ability of Pb^{2+} and Tb^{3+} toward RNA backbone provides a useful method to resolve the secondary structure of RNA (*21*−*25*) based on their preferential accessibility to structurally relaxed regions, such as loops and bulges. However, this property is condition-dependent: When Pb^{2+} or Tb^{3+} cleavage was employed in the presence of an excess amount of competing divalent metal ion such as Mg^{2+}, the cleavage sites were largely consistent with secondary structure, where the structurally accessible sites are generally cleaved (*26*−*29*). On the other hand, low concentrations of Pb^{2+} or Tb^{3+} in the absence or limited amount of competing divalent metal ion tend to induce cleavage at significantly different sites from those observed for the former condition. It has been shown that these sites closely overlap with the divalent metal binding sites resolved in X-ray structures of RNAs (*21*, *28*, *30*, *31*). Thus, Pb^{2+} and Tb^{3+} cleavage sites can be used to approximate the locations of high affinity metal binding sites in an RNA structure (*26*−*28*, *30*−*32*). To identify the Mg^{2+} binding site-(s), we have employed a series of Pb^{2+}- and Tb^{3+}-dependent cleavages of AD02 in the presence of various concentrations of Mg^{2+}.

As discussed above, the Pb^{2+} and Tb^{3+}-dependent cleavage experiments shed insights into two aspects of RNA structure: (i) structurally accessible sites by the hydrolytic metal ions, e.g., single-stranded regions such as bulges and loops, and (ii) high affinity metal binding sites. With the aim of distinguishing the cleavage sites in regard to these two distinct aspects, we first carried out the experiments in the presence of 100 mM Mg^{2+} and various concentrations of Pb^{2+} or Tb^{3+}. With 100 mM Mg^{2+} the ribozyme should fold into its active tertiary structure, and an excess Mg^{2+} over Pb^{2+} or Tb^{3+} would compete for high affinity metal binding sites. Therefore, the observed cleavage profile should mainly represent the structurally accessible sites.

In the Pb^{2+}-induced cleavage profile (Figure 4A), the cleavage occurred predominantly in single-stranded regions,

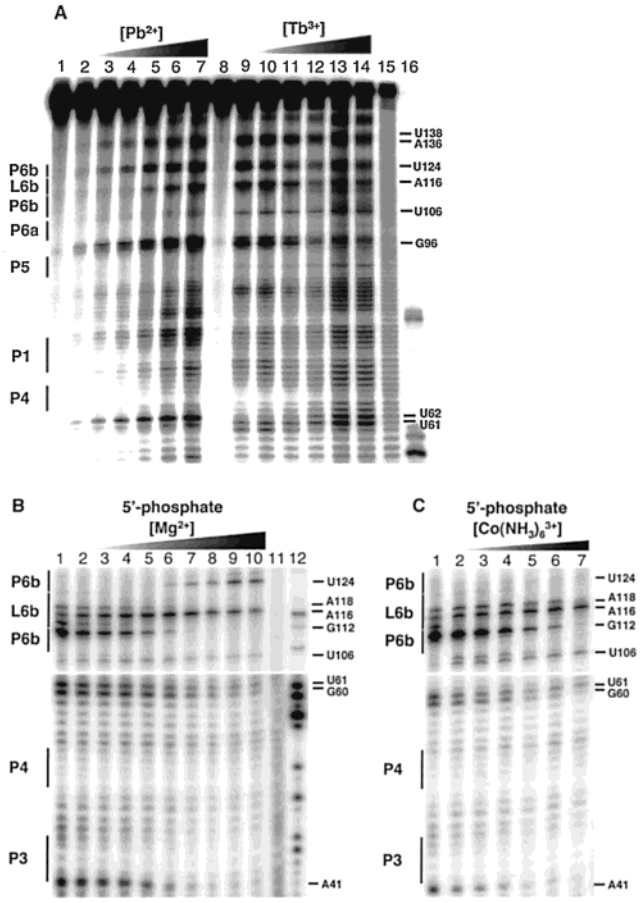

FIGURE 4: Pb^{2+} and Tb^{3+} cleavage profiles of AD02. (A) Cleavage of 5′-[^{32}P]-labeled AD02 in the presence of 100 mM Mg^{2+}. Lanes 1−7 and 8−14 represent the cleavage profiles incubated at the following concentrations of Pb^{2+} and Tb^{3+}, respectively: 0, 0.03, 0.06, 0.12, 0.25, 1, and 2 mM. Lanes 15 and 16 represent an alkaline hydrolysis and T1 ladders, respectively. Cleaved residues were determined based on independent mapping experiments using T1, T2, and S1 nucleases. (B) Cleavage of 5′-[^{32}P]-labeled AD02 in the presence of 50 μM Tb^{3+} as progressively increasing Mg^{2+}. Lanes 1−10 represent the cleavage profiles incubated at the following concentrations of Mg^{2+}: 0, 0.39, 0.78, 1.56, 3.12, 6.25, 12.5, 25, 50, and 100 mM. Lanes 11 and 12 represent an alkaline hydrolysis and T1 ladders, respectively. (C) Cleavage of 5′-[^{32}P]-labeled AD02 in the presence of 50 μM Tb^{3+} as progressively increasing $Co(NH_3)_6^{3+}$. Lanes 1−7 represent the cleavage profiles incubated at the following concentrations of $Co(NH_3)_6^{3+}$: 0, 0.03, 0.06, 0.12, 0.25, 0.5, and 1 mM.

L4, J5−6a, and J6a−7, when Pb^{2+} was present below 0.25 mM (lanes 2−5). The only exception are the cleavages observed at U124 and U125 in P6b, which are in the essential region for the QR domain (vide infra). Above 1 mM Pb^{2+} (lanes 6 and 7), a strong cleavage at A116 in L6b and nonspecific cleavages in P1 and IGS began to appear. Low concentrations of Tb^{3+}-induced cleavages at virtually identical sites as those observed under the low Pb^{2+} conditions, while high concentrations yielded more nonspecific cleavage sites than those witnessed using Pb^{2+}. Nonetheless, the nearly identical cleavage profiles observed for low concentrations of Pb^{2+} and Tb^{3+} indicate that the probed regions are structurally accessible sites.

Although the overall cleavage profiles between Pb^{2+} and Tb^{3+} are similar, minor differences in the cleavage sites were observed: Pb^{2+} cleaves both G96 and U97, while Tb^{3+} specifically cleaves G96. Similarly, Pb^{2+} cleaves both U124 and U125, whereas Tb^{3+} specifically cleaves U124. In the case of Tb^{3+}, mild but specific cleavage was observed at U106 in J6a−6b. These results might be attributed to differences in the physical properties between Pb^{2+} and Tb^{3+} in size and electrostatic strength; the ionic radii of their hexahydrate form are 1.19 and 0.92 Å (*33*), respectively, and Tb^{3+} has a greater electrostatic strength than Pb^{2+}. With the consideration of exploring the high affinity Mg^{2+} binding site, Tb^{3+} seems to be more appropriate choice over Pb^{2+} as a probing reagent because of its smaller size (which is closer to 0.72 Å of Mg^{2+}), its ability to cleave at lower concentrations and higher specificity toward cleavage in certain sites. Therefore, our further studies focused on Tb^{3+} cleavage.

The 5′-[^{32}P]-labeled ribozyme was folded by our standard protocol in the presence of 50 mM K^+ and subjected to the Tb^{3+} cleavage in the absence of Mg^{2+} (Figure 4B, lane 1). Several notable differences were observed in comparison with the profile obtained with 100 mM Mg^{2+} (lane 10): the cleavages at A116 and U124 were no longer pronounced, while G112 was strongly cleaved along with weak cleavages at A118 and A114 (lane 1). The titration of Mg^{2+} ion seems to display a biphasic cleavage profile. In the first phase, the addition of Mg^{2+} leads to a gradual decrease in cleavage at G112, A118, and A114 (lanes 2−6). It also leads to an increase of A116 cleavage up to 6.25 mM (lanes 2−6). In the second phase, further addition of Mg^{2+} induces the cleavage of U124, while the cleavage at A116 remains the same (lanes 7−10). The Mg^{2+}-dependent behavior of these sites is in stark contrast to the Mg^{2+}-independent behavior of U106 (lanes 1−10) as well as G96−A98 and A136−U138 (data not shown), all of which appeared to be structurally accessible sites (*7*). Importantly, the half-maximal Mg^{2+} concentration for the decrease of G112 cleavage, which is approximately 6 mM (lane 4), appears to correlate with its increase of A116 cleavage, suggesting that these two residues are likely communicating. In contrast, the half-maximal Mg^{2+} concentration that induces the U124 cleavage is 30−40 mM (between lanes 8 and 9). In light of the above observations in biphasic cleavage profiles, we hypothesize that there are two Mg^{2+} binding sites in the QR domain: The first Mg^{2+} ion binds strongly to the G112/A116 region (hereafter, this site is referred to as the high affinity metal binding site), resulting in the structural stabilization (or alteration) of the G112−A118 region. The second Mg^{2+} ion, whose binding site is yet undetermined (thereafter, this site is referred to as the low affinity metal binding site), plays a role in the structural alteration observed for the U124 site (*7*).

It should be noted that the critical roles of G112, A116, and U124 in catalysis have been ascertained in previous biochemical analyses (*7*). The mutation of G112 to A or its substitution with inosine in nucleotide analogue interference mapping (NAIM) had detrimental effect on ribozyme activity. Similarly, the substitution of A116 with 7-deazaadenosine and purine riboside as well as the U124C mutation and 5-methyluridine substitution by NAIM strongly interfered the activity. Since the characteristic of the cleavages at these three bases is clearly Mg^{2+}-dependent (Figure 4B), their critical catalytic roles must be governed by Mg^{2+} binding to the G112 site.

We also observed two notable cleavage sites in the ATRib domain, A41 and G60−U61. Both sites showed Mg^{2+}-dependent behavior, where the addition of Mg^{2+} diminishes

Table 1: Relative Rates of 5′-glutaminylation for ATRib Mutants

position	mutation[a]	relative activity[b]
P3	U42c	0.81
P1	U75c/U76c	0.76
L2	U1A	0.98
L4	U61a/U62 g	0.09
	uacg	0.29

[a] See Figure 1A for the structure and position of mutations. [b] The relative rate of each mutant was determined by the comparison of its k_{obs} with the wild type, $k_{obs} = 4.8 \times 10^{-2}$ min^{-1}, in the presence of 100 mM Mg^{2+} in EK buffer.

the cleavage intensity. Our extensive Pb^{2+} and Tb^{3+} studies on ATRib^{trans} (*11*) have suggested that the A41−U42 site forms the Mg^{2+} binding site in concert with the tandem G:U base pairs (G1−G2/U75−U76). The Mg^{2+}-dependent inhibition of the A41 cleavage can be attributed to the Tb^{3+}−Mg^{2+} competition at this site. On the other hand, the G60−U61 cleavage decreases by the addition of Mg^{2+} but does not completely disappear even after the addition of 100 mM Mg^{2+}. It should be noted that elevation of the Tb^{3+} concentration resulted in a gradual increase of the cleavage along with a change of the cleavage site from G60−U61 to U61−U62 (the former trend was also observed for Pb^{2+} cleavage at U62), in stark contrast to the observation that the cleavage of G112 remained protected (Figure 4A). Therefore, the Mg^{2+}-dependent inhibition of the G60−U62 cleavage likely represents a Mg^{2+}-dependent tertiary structural interaction with a certain structural motif(s).

The experiments performed thus far have suggested the presence of three independent metal ion binding sites in AD02. We propose that these sites are located in (i) P3 A41−U42 and P1 G1−G2/U75−U76 in the ATRib domain, based on the results described in the preceding paper in this issue (*11*), and (ii) two metal binding sites in the QR domain, one of which (high affinity metal binding site) is the G112/A116 site and the other of which (low affinity metal binding site) is unknown. If the above hypothesis is correct, mutations that disrupt the Mg^{2+} binding site for the ATRib domain should not affect the QR activity, and vice versa. We have previously demonstrated that two catalytic domains of AD02 can be disconnected to afford ATRib^{trans} and QRtrans (Figure 1A), and this QRtrans can act as a trans-glutaminylation catalyst for ATRib^{trans} (*7*). Since this trans-acting function of QRtrans greatly facilitates the studies for structure−function relationship between two domains, we mainly used this trans-acting catalytic system to verify our hypothesis above.

Two mutants of ATRib^{trans}, P3 U42c and P1 U75c/U76c, were tested for QRtrans-catalyzed glutaminylation (Figure 1A). These mutations were shown to be detrimental for acyl-transfer activity of ATRib^{trans} likely due to the disruption of Mg^{2+} binding (*11*). In contrast, these mutants were active in QRtrans-catalyzed glutaminylation activity, resulting in only mild reduction of activity as compared to the wild-type ATRib^{trans} (Table 1). The observed mild reduction in activity is presumably due to a slight structural change of the 5′-aminoacylation site since both bases are known to constitute the catalytic site of ATRib domain that shares the same 5′-aminoacylation site. These observations agree with the view that QRtrans (or QR domain) has independent metal binding sites from that of ATRib^{trans} (or ATRib domain). We also tested QRtrans-catalyzed glutaminylation of three mutants of ATRib^{trans}, L2 U1A, L4 U61a/U62g, and L4 uacg (Figure 1A), all of which were known to retain the full ATRib activity (*11*). Interestingly, QRtrans glutaminylated the former mutant as well as the wild-type ATRib^{trans}, whereas the glutaminylations on the latter two mutants displayed appreciable reduction of activity as compared to the wild-type (Table 1). These mutations in L4 should not change the structure of the 5′-aminoacylation site of ATRib domain, unlike the L3 and P1 mutations. As discussed earlier, the G60−U62 site is postulated to be involved in Mg^{2+}-dependent tertiary structural interactions. Therefore, the mutations in L4 might disrupt an important tertiary contact with the QRtrans ribozyme to cause significant reduction in trans-glutaminylation.

On the other hand, the G112A mutation in P6b was detrimental for the QR activity in both cis and trans (*7*), but this mutation did not interfere with the acyl-transfer activity of the ATRib domain in AD02 (cis-acting G112A AD02 mutant) or ATRib^{trans} in the presence of QRtrans (data not shown). These observations are consistent with the view that the QR domain has metal binding sites independent from the ATRib domain.

$Co(NH_3)_6^{3+}$ Inhibits the QR-Dependent Glutaminylation. Previously, we reported that ATRib^{trans} functions with $Co(NH_3)_6^{3+}$ as proficiently as with Mg^{2+} (*10*). This has provided concrete evidence that the catalytic Mg^{2+} in ATRib^{trans} is a hydrated form, $Mg^{2+}(H_2O)_6$, that interacts with catalytic residues via outersphere water ligands. Since the Mg^{2+}-dependent kinetics and Tb^{3+}−Mg^{2+}competition cleavage experiments on AD02 have suggested an independent metal binding site present in each catalytic domain, we wondered whether $Co(NH_3)_6^{3+}$ could function for the QR activity. If the QR activity were not supported by $Co(NH_3)_6^{3+}$, the view of independent metal binding sites in QR would be further strengthened. To obtain a general idea of how AD02 behaves in the presence of these two metal ions, we first tested the ATRib and QR activities of AD02 in the presence of $Co(NH_3)_6^{3+}$ or in the presence of both $Co(NH_3)_6^{3+}$ and Mg^{2+}.

The results were quite disparate: The ATRib activity was sustained with $Co(NH_3)_6^{3+}$ and synergistically enhanced by the presence of both metals as expected, whereas the QR activity was inactive with $Co(NH_3)_6^{3+}$ and reduced by the presence of both metals (data not shown). The latter observation suggests that $Co(NH_3)_6^{3+}$ acts as an inhibitor for the QR activity. To gain more insights into the inhibitory effect of $Co(NH_3)_6^{3+}$ for the QR activity, the Mg^{2+}-stimulated self-glutaminylation rate was measured in the presence of various concentrations of $Co(NH_3)_6^{3+}$ (Figure 5). As expected, $Co(NH_3)_6^{3+}$ is a strong inhibitor for the QR activity, giving an inhibition constant of approximately 4 mM for 50 mM Mg^{2+}. This phenomenon can be explained by two scenarios: $Co(NH_3)_6^{3+}$ competes with the essential Mg^{2+} for the same site (either the high or low affinity metal site, or possibly both sites), but slow exchange rate of ligands of $Co(NH_3)_6^{3+}$ prohibits the formation of active state of the catalytic core of QR domain, i.e., the QR domain requires a metal ion that is able to coordinate with the catalytic residues via innersphere interaction. Alternatively, $Co(NH_3)_6^{3+}$ could bind to an independent metal binding site and thereby causes a structural change from the catalytically active form to an inactive conformation.

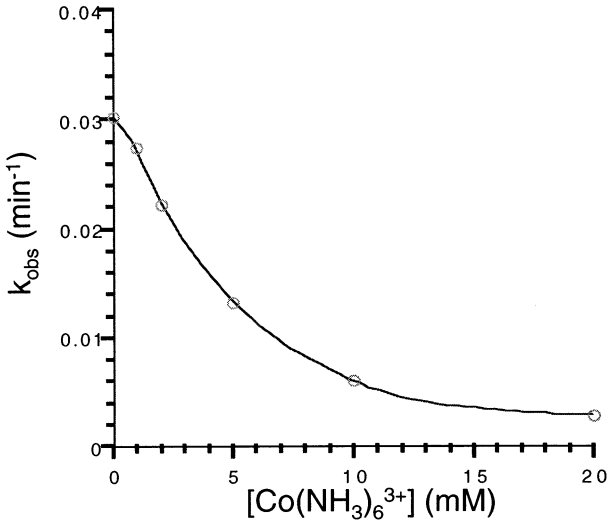

FIGURE 5: $Co(NH_3)_6^{3+}$ inhibition of the QR activity. The observed rate constants (k_{obs}) of QR activity in the presence of 50 mM Mg^{2+} were determined by measuring the initial rates of self-glutaminylation of AD02 (cis-acting) in the presence of various concentrations of $Co(NH_3)_6^{3+}$.

To resolve these two distinct inhibitory mechanisms, we have carried out the Tb^{3+}-induced cleavage by competing with $Co(NH_3)_6^{3+}$ instead of Mg^{2+} (Figure 4C). The cleavage profile by the $Co(NH_3)_6^{3+}$ competition was nearly identical to that observed for the Mg^{2+} competition, except that no cleavage at U124 was observed in elevated concentrations of $Co(NH_3)_6^{3+}$. It should be recalled that the $Tb^{3+}-Mg^{2+}$ competition displayed biphasic cleavage profiles (Figure 4B), where the competition at the high and low affinity metal binding sites were unveiled in the first (lanes 1−5) and second (lanes 6−10) phases, respectively. The observed profiles in the first phase for both $Tb^{3+}-Mg^{2+}$ (Figure 4A, lanes 1−5) and $Tb^{3+}-Co(NH_3)_6^{3+}$ (Figure 4B, lanes 1−5) competitions were identical, suggesting that the high affinity metal binding site is an outersphere metal binding site. On the other hand, the lack of U124 cleavage in the presence of $Co(NH_3)_6^{3+}$ during the second phase (lanes 6−7) indicates that the induction of U124 cleavage is dependent upon the presence of an innersphere metal ion. It should be noted that $Co(NH_3)_6^{3+}$ does not support catalysis, rather acts as a strong inhibitor for the QR activity. This is consistent with the observation that $Co(NH_3)_6^{3+}$ can display the same degree of inhibition of Tb^{3+} cleavage as Mg^{2+} at 10-fold lower concentrations. On the basis of above results, we speculate that the binding of $Co(NH_3)_6^{3+}$ to the high affinity metal binding site may inhibit the subsequent binding of Mg^{2+} to the low affinity metal binding site. Alternatively (or at the same time), $Co(NH_3)_6^{3+}$ may bind to the low affinity metal binding site or nearby, preventing Mg^{2+} from binding to this site. Although this is our favorable hypothesis for the mechanism of $Co(NH_3)_6^{3+}$ inhibition that is also consistent with further analysis of $Tb^{3+}-Mg^{2+}$ and $Tb^{3+}-Co(NH_3)_6^{3+}$ competition experiments using 3′-[^{32}P]-labeled ribozymes (vide infra), we cannot completely rule out the possibility that $Co(NH_3)_6^{3+}$ allosterically inhibits the QR activity by binding to metal binding sites different from the Mg^{2+} binding sites. Nonetheless, the above results suggest that the innersphere metal ion is essential for activity presumably in the relation to the structural alteration of P6b (vide infra),

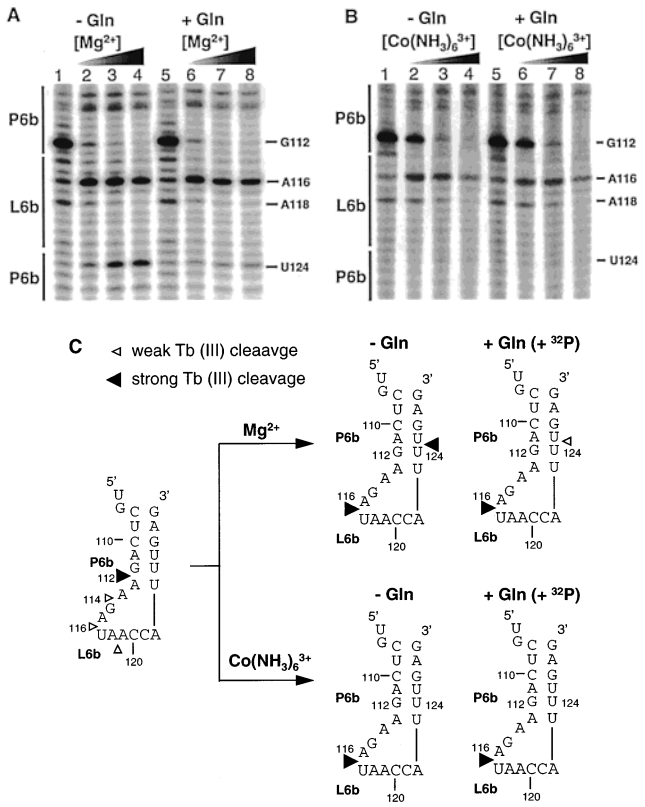

FIGURE 6: Tb^{3+} cleavage competing with Mg^{2+} or $Co(NH_3)_6^{3+}$ of 5′-OH- or 5′-Gln-AD02. (A) Cleavage of 3′-[^{32}P]-labeled AD02 in the presence of 50 μM Tb^{3+} in the presence of Mg^{2+}. Lanes 1−4 and 5−8 represent two sets of samples in the absence and presence of 5 mM biotin-L-Gln-CME, respectively. Both sets were titrated with following Mg^{2+} concentration: 0, 10, 20, and 30 mM. (B) Cleavage of 3′-[^{32}P]-labeled AD02 in the presence of 50 μM Tb^{3+} in the presence of $Co(NH_3)_6^{3+}$. Lanes 1−4 and 5−8 represent two sets of samples in the absence and presence of 5 mM biotin-L-Gln-CME, respectively. Both sets were titrated with following $Co(NH_3)_6^{3+}$ concentration: 0, 0.1, 0.5, and 1 mM. (C) Schematic representation of Tb^{3+} cleavage profiles in the region of P6b−L6b derived from Mg^{2+} and $Co(NH_3)_6^{3+}$ competition experiments in the absence and presence of biotin-L-Gln-CME. Strong (filled) and weak (open) Tb^{3+} cleavage sites are indicated by triangles.

which was previously supported by a number of biochemical mapping studies (*7*).

Essential Roles of Innersphere Metal Ions in the QR Domain. Our previous CMCT modification of the AD02 ribozyme showed that U125 is exposed to solvent, i.e., bulged out, only when 5′-OH group was glutaminylated (*7*). In addition, Pb^{2+} cleavage at U124 in the presence of 100 mM Mg^{2+} is protected by the 5′-glutaminylation (*7*). These results imply that a dynamic change of the P6b configuration, in particular at U124−U125, occurs after 5′-glutaminylation. No Tb^{3+} cleavage at U124 in the presence of $Co(NH_3)_6^{3+}$ suggests that the above structural change may be a specific event for an innersphere metal ion.

Since the series of Tb^{3+} cleavage experiments described above were done with 5′-[^{32}P]-labeled AD02, this system does not allow us to detect the effect of 5′-glutaminylation on the Tb^{3+} cleavage. It is also possible that 5′-phosphorylated ribozyme acts differently from 5′-OH- or 5′-Gln-ribozyme. We therefore constructed a 3′-[^{32}P]-labeled AD02 ribozyme and investigated Tb^{3+}-dependent cleavage competing with Mg^{2+} using 5′-OH- or 5′-Gln-ribozyme (Figure 6A). The cleavage profiles of these two forms of ribozyme were

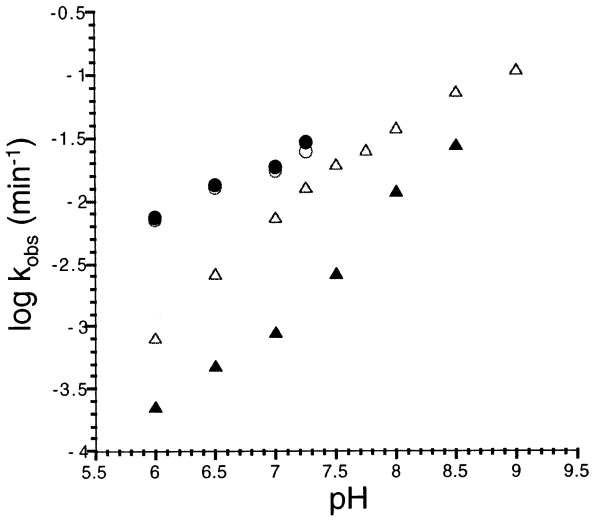

FIGURE 7: pH-dependence of the QR activity. Cis-reactions were carried out in the presence of 50 mM Mg^{2+} (open triangles), 20 mM Ca^{2+} (filled triangles), 10 mM Mg^{2+} (open circles), or 10 mM Ca^{2+} (filled circles). For the pH-dependent kinetics performed with 10 mM Mg^{2+} or Ca^{2+}, 2 mM spermidine was added in the reaction.

virtually the same as those observed for 5′-[^{32}P]-ribozyme at most cleavage sites, except that the cleavage at U124 was more pronounced in the case of 5′-OH-ribozyme than the 5′-Gln-ribozyme. The top panel of Figure 6C summarizes the cleavage profiles observed for 5′-OH and 5′-Gln-ribozymes in the absence and presence of Mg^{2+}. These cleavage profiles are also consistent with those observed for Pb^{2+}-induced cleavage reported previously (*7*). The results thus suggest that the U124 site is more accessible to Tb^{3+} cleavage in the 5′-OH ribozyme than the 5′-Gln-ribozyme and also imply that the 5′-[^{32}P]-ribozyme is a structural form analogous to the 5′-Gln-ribozyme.

We next employed $Tb^{3+}-Co(NH_3)_6^{3+}$ competition cleavage experiment with 5′-OH-ribozyme. The observed cleavage profile was identical to that observed for 5′-[^{32}P]-ribozyme (Figure 6B), in which no U124 cleavage was observed (Figure 6C, bottom panel). Since the ribozyme is unable to glutaminylate the 5′-OH group in the presence of $Co(NH_3)_6^{3+}$, it is expected to see no change in the cleavage profile in the presence of the Gln substrate (Figure 6B). However, the 5′-[^{32}P]-ribozyme should have an analogous structural form to the 5′-Gln-ribozyme. Therefore, our earlier observation for no Tb^{3+} cleavage at U124 in the presence of $Co(NH_3)_6^{3+}$ using the 5′-[^{32}P]-ribozyme suggests that $Co(NH_3)_6^{3+}$ is unable to induce the same structural change as Mg^{2+} in the either form of ribozyme (5′-OH or 5′-Gln). Thus, we conclude that the catalytic inability of $Co(NH_3)_6^{3+}$ for the QR activity is most likely due to its lack of ability to alter the configuration of P6b. The largest difference in properties of $Mg^{2+}(H_2O)_6$ from $Co(NH_3)_6^{3+}$ is the ability of ligand exchange. Therefore, the formation of an innersphere complex of Mg^{2+} with the catalytic residues in the metal binding sites probably induces the structural alteration of P6b, thus resulting in constitution of the Gln binding site.

pH-Dependent Activity of Self-Glutaminylation. To gain more insights into the roles of metal ion in the QR activity, kinetic assays were carried out under variable pH conditions either with 50 mM Mg^{2+} or 20 mM Ca^{2+} in AD02 (Figure 7). Plots show a linear hydroxide ion dependence with

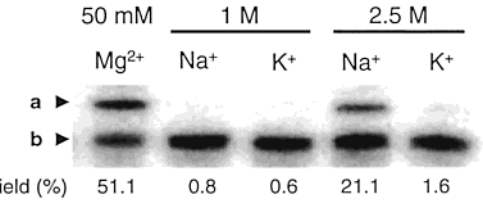

FIGURE 8: The stimulation of QR activity by monovalent ions. Cis-reactions were carried out in 50 mM EPPS, pH 7.5, 1.25 mM EDTA, and either 1 or 2.5 M of NaCl or KCl for 1 h. Lane 1 is the control lane in which reaction was carried out in 50 mM KCl, 50 mM EPPS, pH 7.5, and 50 mM $MgCl_2$. The arrowhead shows: a, biotin-Gln-AD02 complexed with SAv; b, AD02.

increasing pH (although in the case of Mg^{2+} the plot above pH 8 becomes slightly less steep), suggesting that chemistry is rate-limiting for the self-glutaminylation.

We observed earlier in the Mg^{2+} and Ca^{2+} titration experiments that in the presence of spermidine the self-glutaminylation rate is nearly identical between two metal ions when the same concentration was used. We further confirmed this behavior by running pH-dependent kinetics at 10 mM of each divalent metal ion in the presence of 2 mM spermidine (Figure 7). The observed coinciding behavior at low concentration of both metal ions indicates that differences of their chemical properties, such as pK_a of water ligands and ionic radius, are not critical determinants for activity. This suggests that the observed hydroxide-dependent activity is due to a nonmetal hydroxide-dependent species such as a hydroxide ion of the 5′-OH group of ribozyme. We therefore propose that the alkaline earth metal ion necessary for the QR activity unlikely plays a direct role in chemistry but rather plays a critical structural role to constitute the Gln binding site.

Catalytic Activity Supported by Monovalent Ions. The catalytic function of ribozymes often relies on the presence of divalent metal ions (*13*, *18*, *30*−*32*, *34*−*46*), which are argued to be involved directly in chemistry. However, recent studies on hammerhead (*47*−*49*), hairpin (*47*), and VS (*47*) ribozymes have shown that high concentration of monovalent ion alone can support catalysis. Although monovalent ions fail to display an equal activity to that supported by Mg^{2+} or other divalent metal ions, the difference is considerably little in terms of rate acceleration gained by monovalent ion-supported ribozyme catalysis over its uncatalyzed rate. Our recent studies on ATRib^{trans} (*11*) have revealed that Na^+ is a potent inhibitor of Mg^{2+}-supported ATRib activity. However, an excess (2 M) addition of Na^+ can support catalysis with a 10-fold lower activity than the maximal activity under saturating Mg^{2+} conditions. Taken together with other kinetic data, we conclude that the roles of metal ion are both structural and chemical, in which the metal ion helps to constitute the catalytic core motif and simultaneously stabilizes the oxyanion developed in the transition state of acyl-transfer reaction via the outersphere coordination.

As hypothesized, if Mg^{2+} ion in the QR domain plays purely a structural role, we expect that high concentration of monovalent ion should support catalysis. We therefore examined the QR activity in the presence of either NaCl or KCl. Although 1 M Na^+ supports catalysis modestly, 2.5 M Na^+ shows considerable activity where the activity is only 2.4-fold lower as compared to that with 50 mM Mg^{2+} (Figure 8). On the other hand, K^+ is a much poorer substitute for

Mg^{2+} than Na^+, giving very weak activity even at 2.5 M. This difference between Na^+ and K^+ can be explained by a difference of their physical properties, Na^+ is closer in size to Mg^{2+} than K^+. However, the requirement of high concentrations of Na^+ ion provides only ambiguous support for our hypothesis, since this can be explained by two possible scenarios (i.e., supporting or opposing our hypothesis): Na^+ ion has a much weaker affinity to the metal binding site compared to Mg^{2+} due to its weaker electrostatic strength, thereby requires high concentrations for binding. Alternatively, monovalent ion can act as an inhibitor (i.e., it can bind well to the Mg^{2+} binding site but cannot support catalysis at low concentrations due to its weaker electrostatic strength), but supports catalysis at high concentrations via an unknown mechanism, similar to the phenomena observed in $ATRib^{trans}$ (*11*). To resolve these two distinct mechanisms, we measured the QR activity in the presence of 20 mM Mg^{2+} by competing with various concentrations of NaCl (0.5−2 M). The QR activity under these conditions showed no significant change from that observed in the absence of NaCl, except that a modest cooperative enhancement of activity was observed when both 2 M NaCl and 20 mM Mg^{2+} were present (data not shown). This allows us to rule out the second scenario but strongly supports the first scenario. This in turn indicates that the metal binding site in QR domain is highly specific to Mg^{2+}. Thus, the role of Mg^{2+} in QR domain is purely structural, which is probably responsible to trigger the formation of glutamine binding site.

CONCLUSION

Here we have revealed distinct roles of divalent metal ions in the bifunctional AD02 ribozyme. The acyl-transfer activity is supported by both Mg^{2+} and $Co(NH_3)_6^{3+}$, whereas the glutaminylation activity is supported by Mg^{2+} (and Ca^{2+}) but not $Co(NH_3)_6^{3+}$ which rather acts as a strong inhibitor. We have proposed that the former metal ion in the ATRib domain plays both structural and chemical roles, and the latter metal ion in the QR domain plays a purely structural role. The extensive Pb^{2+} and Tb^{3+} cleavage and kinetic studies have revealed that each catalytic domain has independent metal binding sites. The present study shows that two metal binding sites are present in the QR domain. The first site is a high affinity metal binding site most likely composed of the G112/A116 region, and the second site is a low affinity site whose location is not yet determined. The innersphere interaction of metal ion to these binding sites is critical to form the glutamine binding site in the QR domain, in contrast to the requirement of outersphere ligand contacts in the ATRib domain. Thus, the in vitro evolution of ATRib into the more sophisticated AD02 ribozyme (*6*) has added a novel catalytic domain that utilizes a chemical mechanism distinct from the preexisting mechanism. Similar event could have taken place to evolve functionally complex ribozymes, such as splicing ribozymes and ribosomal RNA, from primitive precursor ribozymes in the RNA world (*30*).

The approach utilized in this and the preceding studies (*11*) is a useful means to determine potential high affinity metal binding sites. We believe that this approach is generally applicable to other RNA molecules, as recently demonstrated by Walter et al. in a hairpin ribozyme (*26*), Sigel et al. in a group II intron ribozyme (*27*), and Vaidya et al. in an acyltransferase ribozyme (*29*). The combination of other biochemical methods with this approach would shed further light on diverse roles of metal ions in ribozyme catalysis.

ACKNOWLEDGMENT

N.L. thanks Mark-Diamond Research Fund for generous support. We also thank Anand Vaidya and David Hodgson for critical proof-reading as well as the members of the Suga group for their helpful discussions.

REFERENCES

1. Wilson, D. S., and Szostak, J. W. (1999) *Annu. Rev. Biochemistry 68*, 611−647.
2. Yarus, M. (1999) *Curr. Opin. Chem. Biol. 3*, 260−267.
3. Yarus, M., and Illangasekare, M. (1999) in *The RNA World*, 2nd ed. (Gesteland, R. F., Cech, T. R., Atkins, J. F., Eds.) pp 183−196, Cold Spring Harbor Laboratory Press, Cold Spring Harbor.
4. Bartel, D. P., and Unrau, P. J. (1999) *Trends Cell Biol. 9*, M9-M13.
5. Bartel, D. P. (1999) in *The RNA World*, 2nd ed. (Gesteland, R. F.; Cech, T. R., Atkins, J. F., Eds.) pp 143−162, Cold Spring Harbor Laboratory Press, Cold Spring Harbor.
6. Lee, N., Bessho, Y., Wei, K., Szostak, J. W., and Suga, H. (2000) *Nat. Struct. Biol. 7*, 28−33.
7. Lee, N., and Suga, H. (2001) *RNA 7*, 1043−1051.
8. Lohse, P. A., and Szostak, J. W. (1996) *Nature 381*, 442−444.
9. Suga, H., Lohse, P. A., and Szostak, J. W. (1998) *J. Am. Chem. Soc. 120*, 1151−1156.
10. Suga, H., Cowan, J. A., and Szostak, J. W. (1998) *Biochemistry 37*, 10118−10125.
11. Flynn-Charlebois, A., Lee, N., and Suga, H. (2001) *Biochemistry 40*, 13623−13632.
12. Huang, Z., and Szostak, J. W. (1996) *Nucleic Acids Res. 24*, 4360−4361.
13. Dahm, S. C., and Uhlenbeck, O. C. (1991) *Biochemistry 30*, 9464−9469.
14. Wu, H. N., Lin, Y. J., Lin, F. P., Makino, S., Chang, M. F., and Lai, M. M. (1989) *Proc. Natl. Acad. Sci. U.S.A. 86*, 1831−1835.
15. Collins, R. A., and Olive, J. E. (1993) *Biochemistry 32*, 2795−2799.
16. Smith, D., Burgin, A. B., Haas, E. S., and Pace, N. R. (1992) *J. Biol. Chem. 267*, 2429−2436.
17. Grosshans, C. A., and Cech, T. R. (1989) *Biochemistry 28*, 6888−6894.
18. Dahm, A. C., Derrick, W. B., and Uhlenbeck, O. C. (1993) *Biochemistry 32*, 13040−13045.
19. Chowrira, B. M., Berzal-Herranz, A., and Burke, J. M. (1993) *Biochemistry 32*, 1088−1095.
20. Smith, D., and Pace, N. R. (1993) *Biochemistry 32*, 5273−5281.
21. Krzyzosiak, W. J., Marciniec, T., Wiewiorowski, M., Romby, P., Ebel, J. P., and Giege, R. (1988) *Biochemistry 27*, 5771−5777.
22. Pan, T., Gutell, R. R., and Uhlenbeck, O. C. (1991) *Science 254*, 1361−1364.
23. Zito, K., Huttenhofer, A., and Pace, N. R. (1993) *Nucleic Acids Res. 21*, 5916−5920.
24. Ciesiolka, J., Hardt, W. D., Schlegl, J., Erdmann, V. A., and Hartmann, R. K. (1994) *Eur. J. Biochem. 219*, 49−56.
25. Winter, D., Polacek, N., Halama, I., Streicher, B., and Barta, A. (1997) *Nucleic Acids Res. 25*, 1817−1824.
26. Walter, N. G., Yang, N., and Burke, J. M. (2000) *J. Mol. Biol. 298*, 539−555.
27. Sigel, R. K., Vaidya, A., and Pyle, A. M. (2000) *Nat. Struct. Biol. 7*, 1111−1116.
28. Hargittai, M. R., and Musier-Forsyth, K. (2000) *RNA 6*, 1672−1680.
29. Vaidya, A., and Suga, H. (2001) *Biochemistry, 24*, 7200−7210.

30. Feig, A. L., and Uhlenbeck, O. C. (1999) in *The RNA World*, 2nd ed. (Gesteland, R. F., Cech, T. R., Atkins, J. F., Eds.) pp 287−319, Cold Spring Harbor Laboratory Press, Cold Spring Harbor.
31. Feig, A. L., Scott, W. G., and Uhlenbeck, O. C. (1998) *Science 279*, 81−84.
32. Scott, W. G., Murray, J. B., Arnold, J. R. P., Stoddard, B. L., and Klug, A. (1996) *Science 274*, 2065−2069.
33. Shannon, R. D. (1976) *Acta Crystallogr. A32*, 751−767.
34. Steitz, T. A., and Steitz, J. A. (1993) *Proc. Natl. Acad. Sci. U.S.A. 90*, 6498−6502.
35. Pyle, A. M. (1993) *Science 261*, 709−714.
36. Zhou, D.-M., Zhang, L.-H., and Taira, K. (1998) *Proc. Natl. Acad. Sci. U.S.A. 94*, 14343−14348.
37. Pontius, B. W., Lott, W. B., and von Hippel, P. H. (1997) *Proc. Natl. Acad. Sci. U.S.A. 94*, 2290−2294.
38. Ruffner, D. E., and Uhlenbeck, O. C. (1990) *Nucleic Acids Res. 18*, 6025−6029.
39. Scott, E. C., and Uhlenbeck, O. C. (1999) *Nucleic Acids Res. 27*, 479−484.
40. Piccirilli, J. A., Vyle, J. S., Caruthers, M. H., and Cech, T. R. (1993) *Nature 361*, 85−88.
41. Weinstein, L. B., Jones, B. C., Cosstick, R., and Cech, T. R. (1997) *Nature 388*, 805−808.
42. Shan, S. O., and Herschlag, D. (2000) *RNA 6*, 795−813.
43. Hampel, A., and Cowan, J. A. (1997) *Chem. Biol. 4*, 513−517.
44. Perrotta, A. T., Shih, I.-H., and Been, M. D. (1999) *Science 286*, 123−126.
45. Nakano, S., Chadalavada, D. M., and Bevilacqua, P. C. (2000) *Science 287*, 1493−1497.
46. Christian, E. L., Kaye, N. M., and Harris, M. E. (2000) *RNA 6*, 511−519.
47. Murray, J. B., Seyhan, A. A., Walter, N. G., Burke, J. M., and Scott, W. G. (1998) *Chem. Biol. 5*, 587−595.
48. O'Rear, J. L., Wang, S., Feig, A. L., Beigelman, L., Uhlenbeck, O. C., and Herschlag, D. (2001) *RNA 7*, 537−545.
49. Curtis, E. A., and Bartel, D. P. (2001) *RNA 7*, 546−552.

BI011103C